Electronic Supplementary Information (ESI)

Surface Chiroselective Assembly of Enantiopure Crystalline Porous Films Containing Bichiral Building Blocks

Hao Chen [ac], *Zhi-Gang Gu** [abc] *and Jian Zhang** [abc]

[a] State Key Laboratory of Structural Chemistry, Fujian Institute of Research on the Structure of Matter, Chinese Academy of Sciences, Fuzhou, Fujian 350002, P. R. China

[b] Fujian Science & Technology Innovation Laboratory for Optoelectronic Information of China, Fuzhou, Fujian 350108, P. R. China

[c] University of Chinese Academy of Sciences, Beijing 100049, P.R. China

Address correspondence to zggu@fjirsm.ac.cn and zhj@fjirsm.ac.cn

Table of Contents

Figure S14. The CD liquid-state spectra of (*R*)- and (*S*)-$Mn(DCH)_3$, (*R*)- and (*S*)-DCH in ethanolic solution.
Figure S15. CPL dissymmetry factor (g_{lum}) spectra of (*R*, Δ)- and (*S*, Λ)-CPM films (excitation at 365 nm).
Figure S16. Mass uptakes of *D*- and *L*-methyl lactate in (*R*, Δ)- (a) and (*S*, Λ)-CPM films (b) using by a gas phase QCM technique; Mass uptakes (c) and enantioselectivity (d) of *D*- and *L*-methyl lactate in (*R*, Δ)- and (*S*, Λ)-CPM films.
Figure S17. SEM images (a, b), AFM image (c), SEM EDS (d) and element mapping (e) of (*S*, Λ)-CPM film.
Figure S18. The liquid-state CD spectra of racemic Ti_4L_6 cages in ethanolic solution.

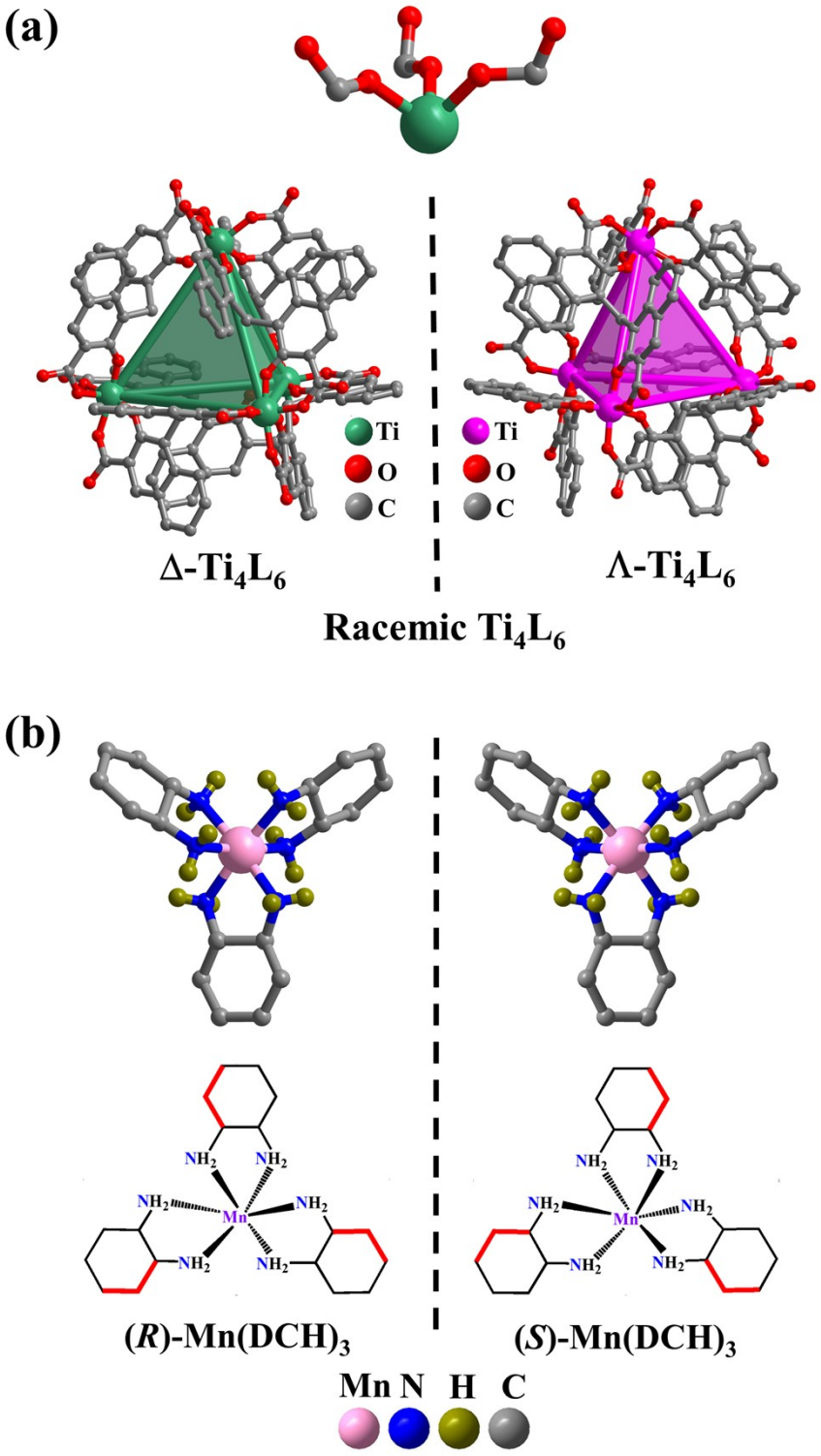

Figure S1. (a) Structures of the Δ-Ti_4L_6 and Λ-Ti_4L_6 isomers in racemic Ti_4L_6 cages; (b) Model structures of the (*R*)- and (*S*)-DCH (DCH = 1,2-diaminocyclohexane) units.

Ti_4L_6 cage with calixarene-like coordination-active vertices has many carbonyl oxygen atoms, which are not coordinated to any metal ions. Such vertex of Ti_4L_6 cage looks like a claw. The Mn-complexs are positive bivalent, and the anion is the CH_3COO^-.

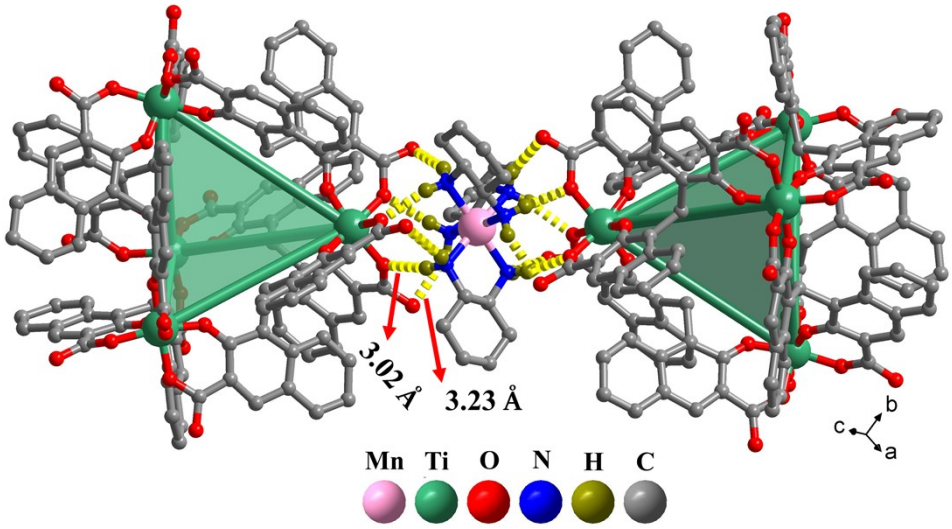

Figure S2. Two adjacent Δ-Ti_4L_6 cages linked by one (*R*)-$Mn(DCH)_3$ unit through N−H···O hydrogen bonds.

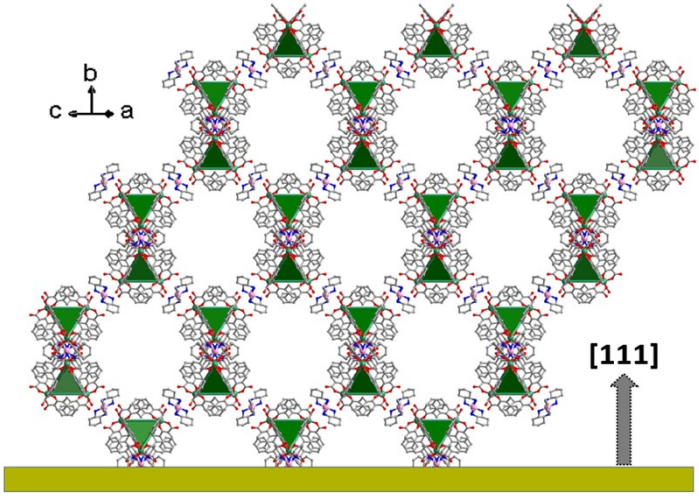

Figure S3. Structures of the (*R*, Δ)-CPM film along [111] orientation.

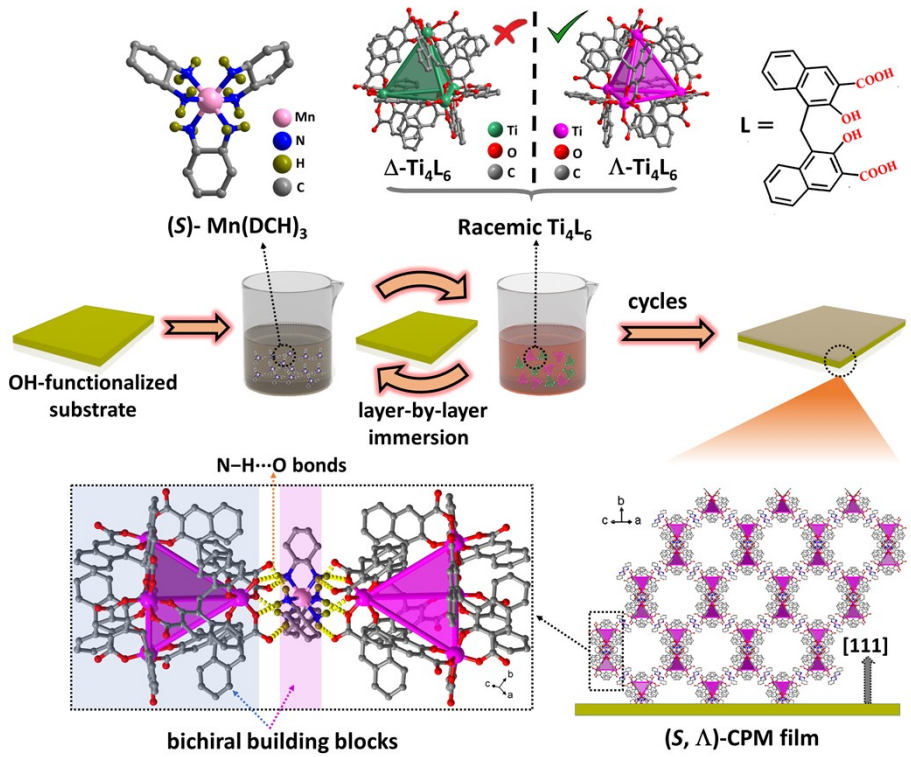

Figure S4. The preparation diagrammatic sketch of (*S*, Λ)-CPM film by the autoarm immersion layer-by-layer assembly method.

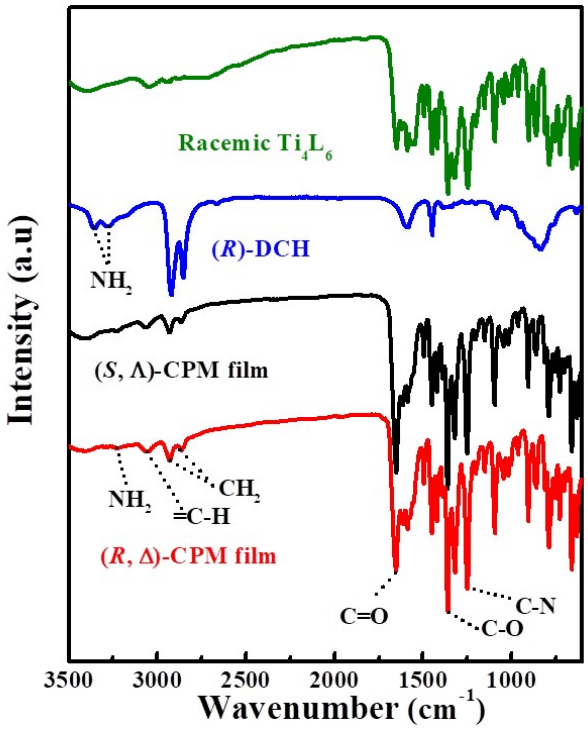

Figure S5. IR spectra of racemic Ti_4L_6, (R)-DCH, (*R*, Δ)- and (*S*, Λ)-CPM films.

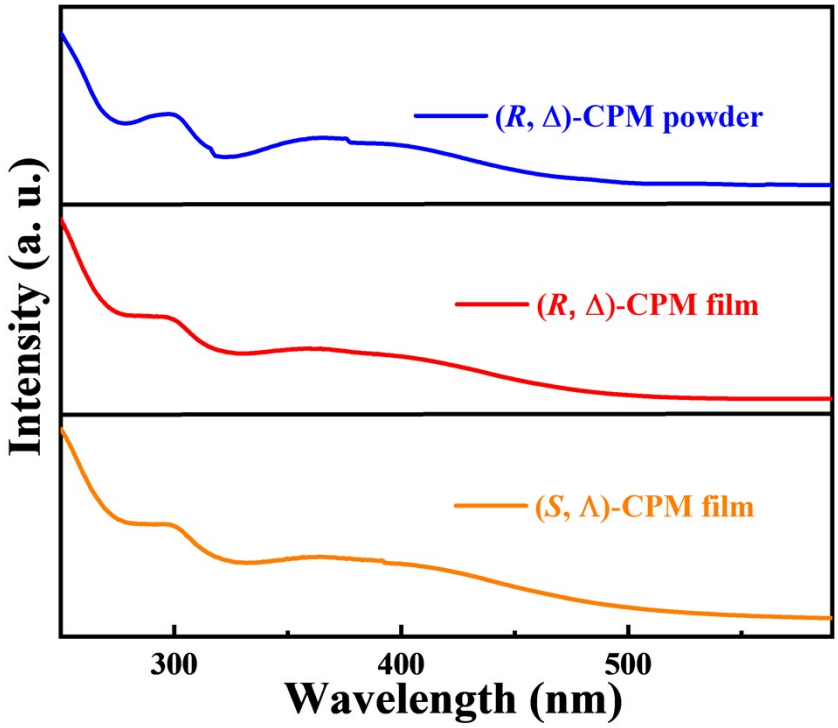

Figure S6. UV-vis spectra of (*R*, Δ)- and (*S*, Λ)-CPM films and powder of (*R*, Δ)-CPM.

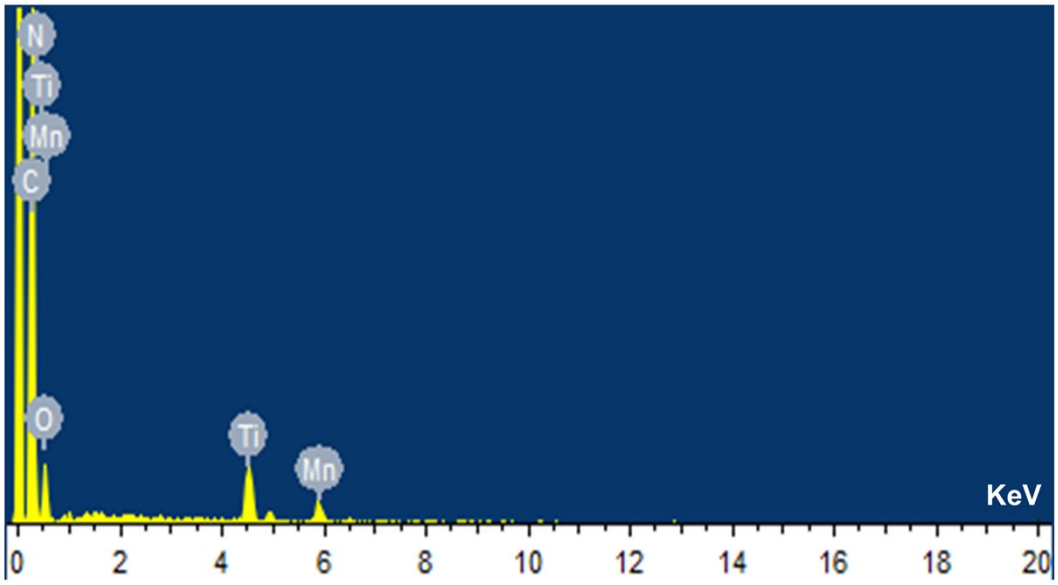

Figure S7. SEM EDS of (*R*, Δ)-CPM film.

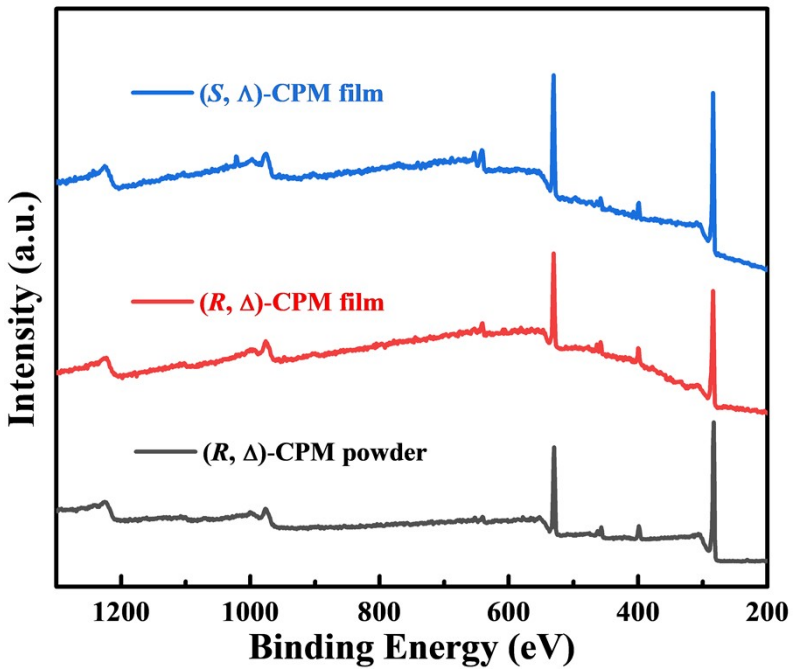

Figure S8. Survey XPS spectra of (*R*, Δ)- and (*S*, Λ)-CPM films and powder of (*R*, Δ)-CPM.

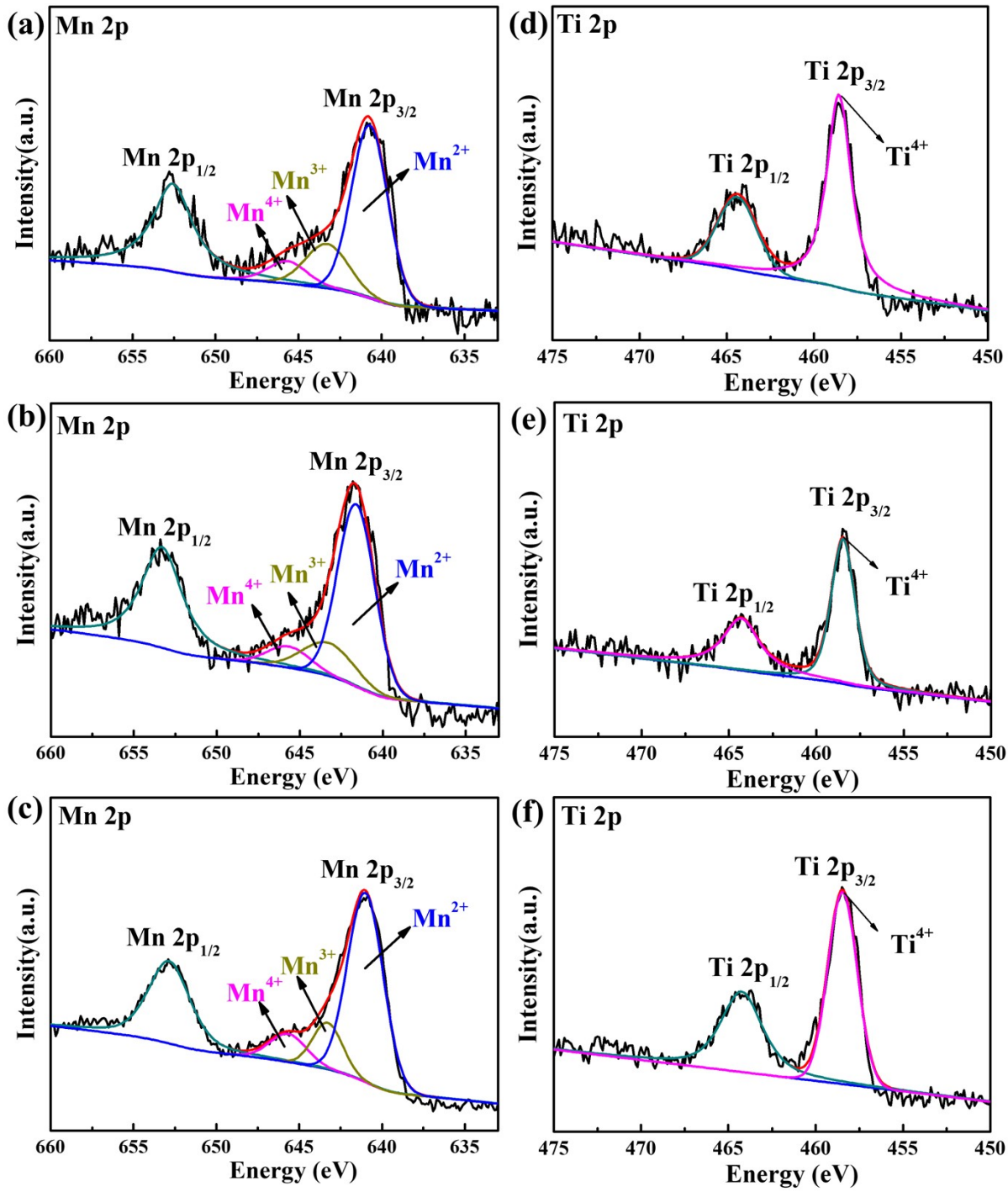

Figure S9. The high resolution of XPS: Mn 2p XPS spectra of (*R*, Δ)-CPM film (a), (*S*, Λ)-CPM film (b), and powder of (*R*, Δ)-CPM (c); Ti 2p XPS spectra of (*R*, Δ)-CPM film (d), (*S*, Λ)-CPM film (e), and powder of (*R*, Δ)-CPM (f).

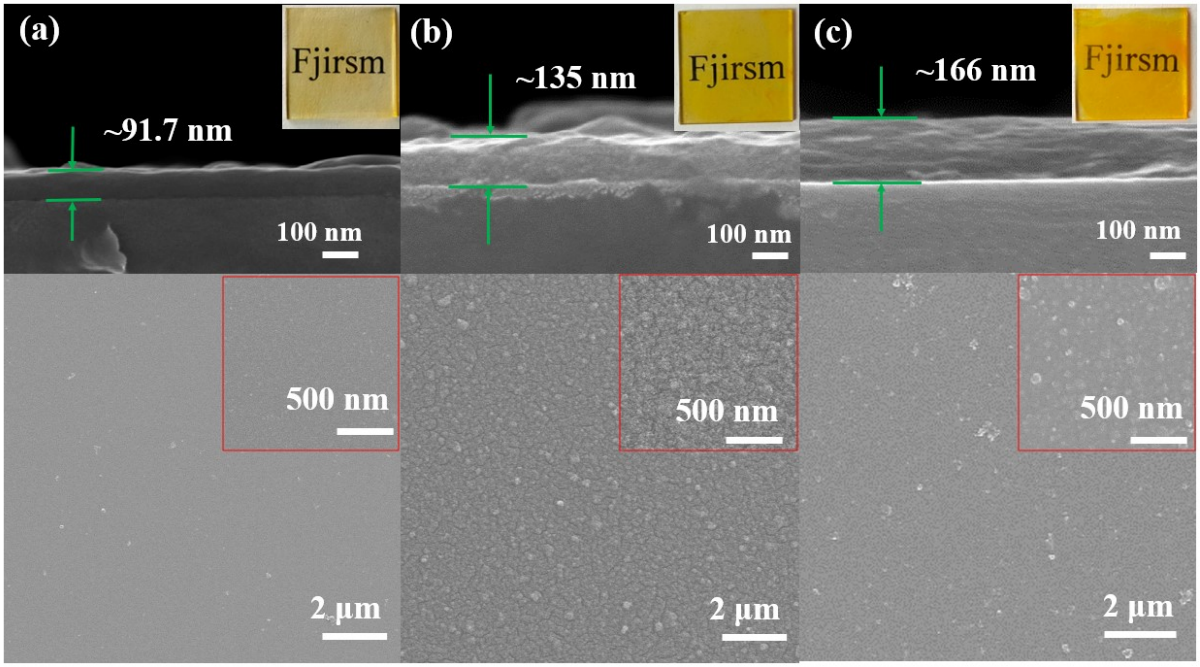

Figure S10. (a) Surface and cross-sectional SEM images of (*R*, Δ)-CPM-20, (*R*, Δ)-CPM-30 (b), and (*R*, Δ)-CPM-40 (c).

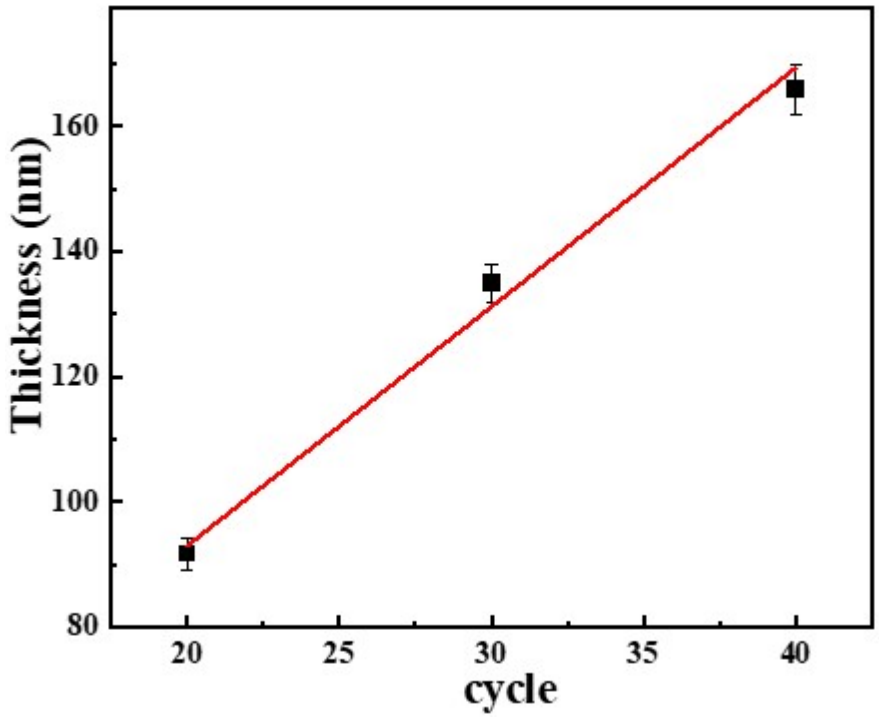

Figure S11. Plot of (*R*, Δ)-CPM film thickness versus preparation cycles.

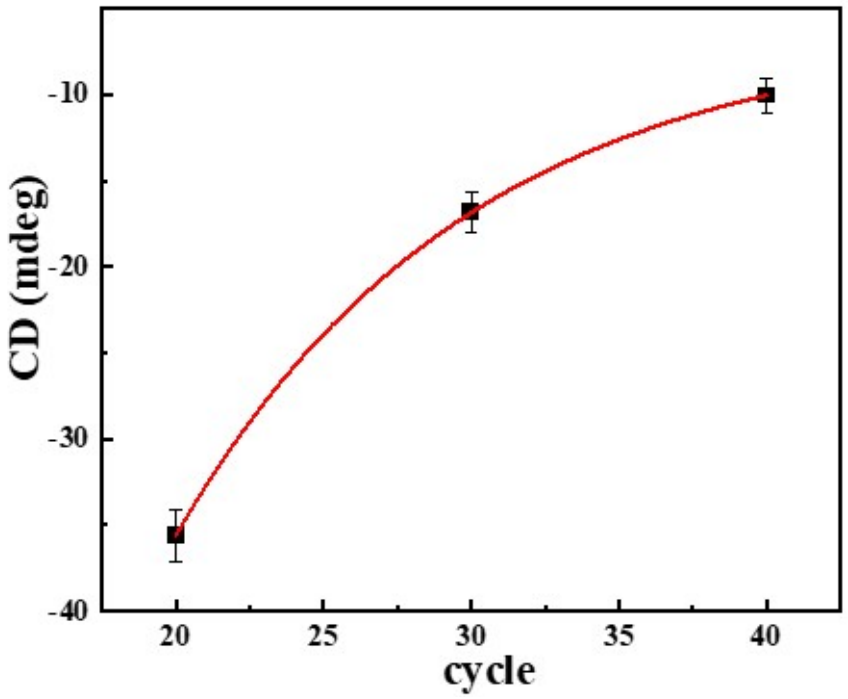

Figure S12. Plot of (*R*, Δ)-CPM film CD peak at 360 nm versus preparation cycles.

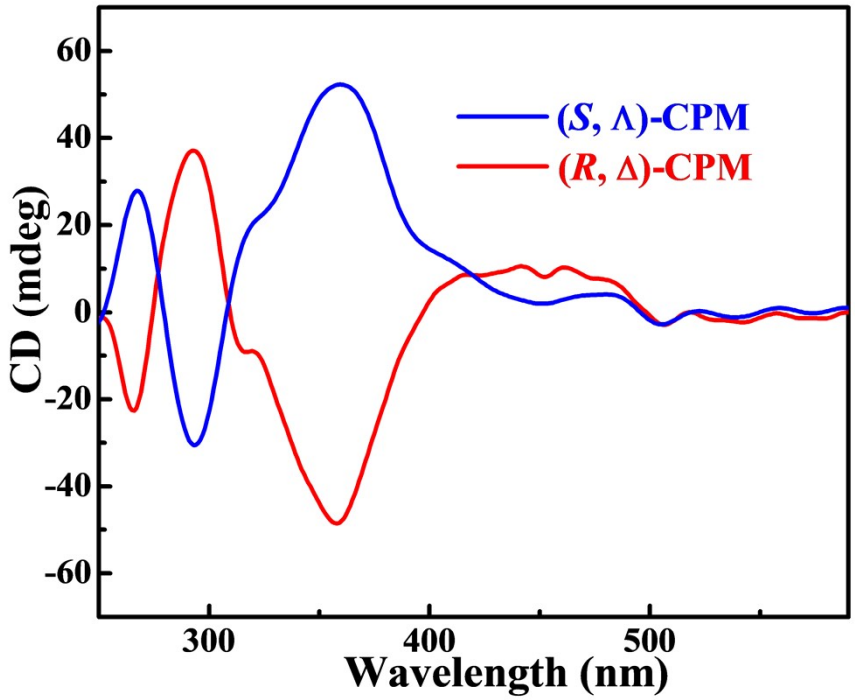

Figure S13. The liquid-state CD spectra of (*R*, Δ)- and (*S*, Λ)-CPM in ethanolic solution.

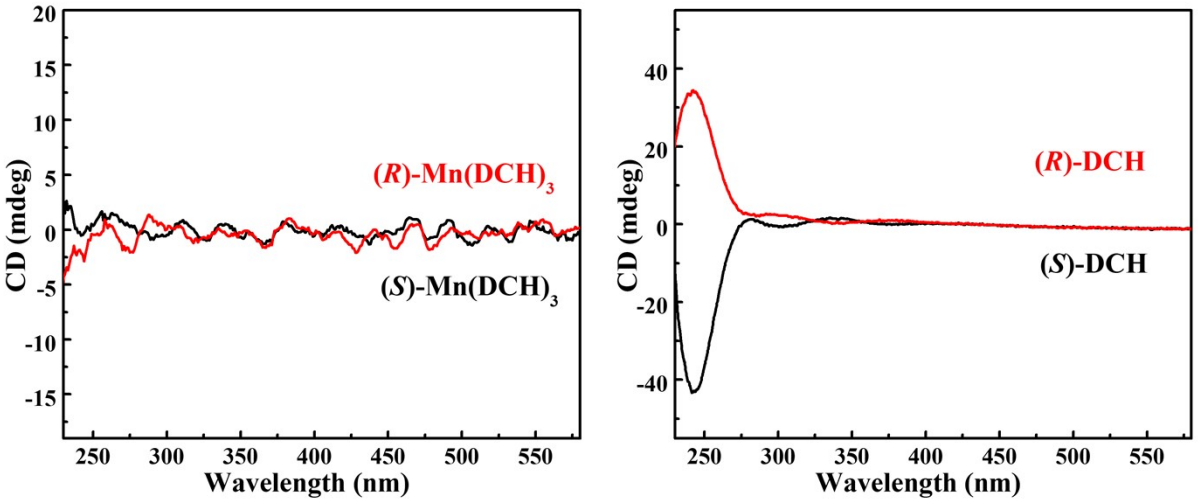

Figure S14. The liquid-state CD spectra of (*R*)- and (*S*)-$Mn(DCH)_3$, (*R*)- and (*S*)-DCH in ethanolic solution.

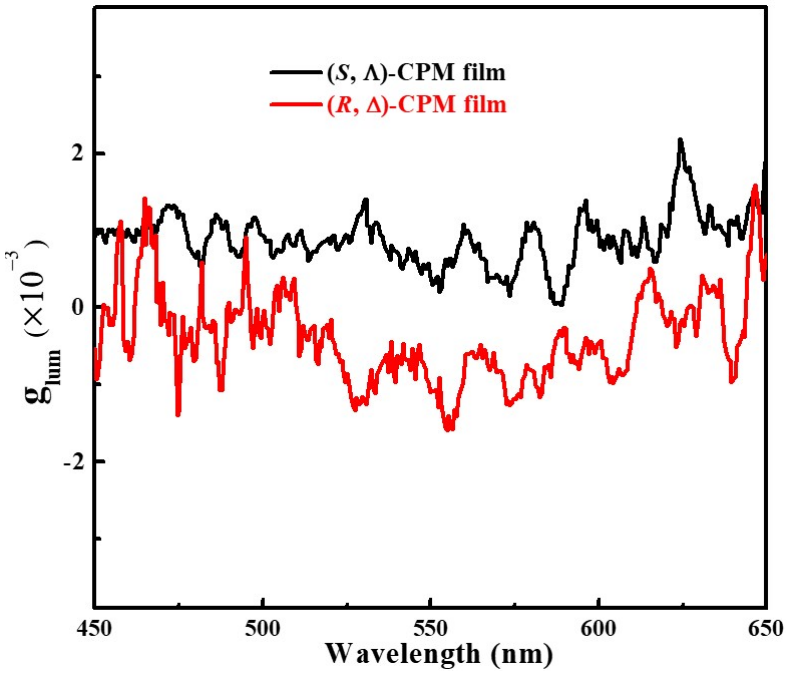

Figure S15. CPL dissymmetry factor (g_{lum}) spectra of (*R*, Δ)- and (*S*, Λ)-CPM films (excitation at 365 nm).

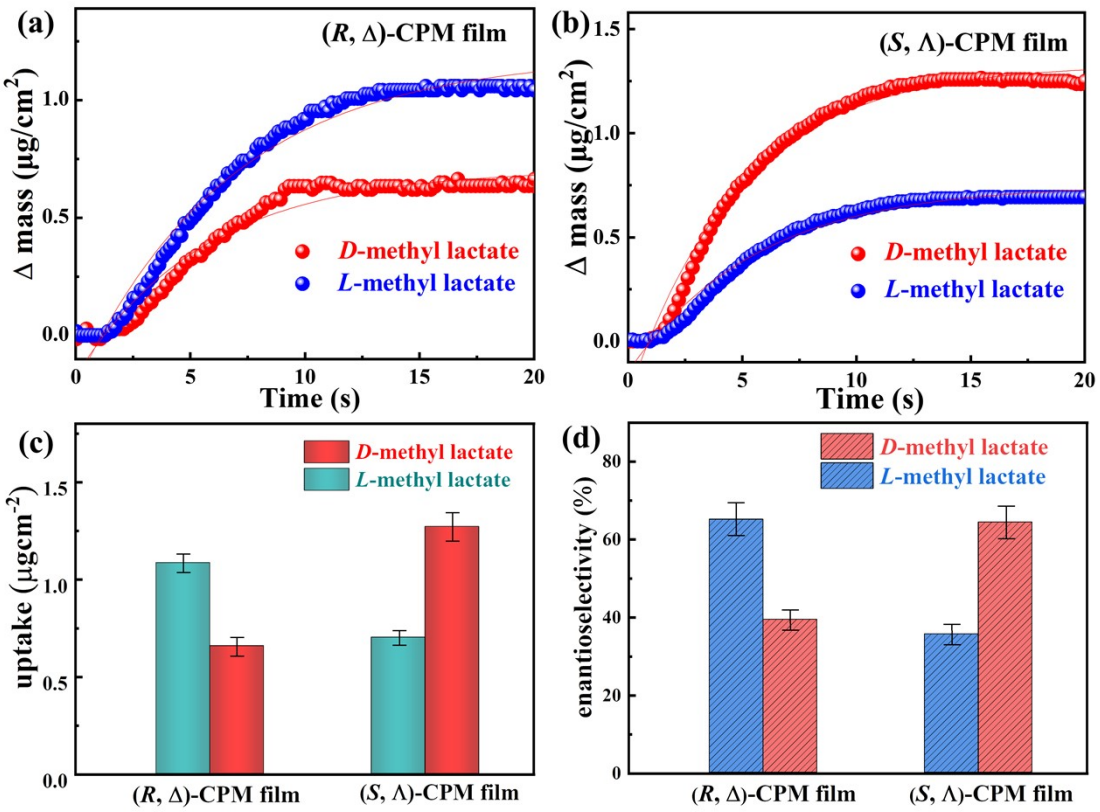

Figure S16. Mass uptakes of *D*- and *L*-methyl lactate in (*R*, Δ)- (a) and (*S*, Λ)-CPM films (b) using by a gas phase QCM technique; Mass uptakes (c) and enantioselectivity (d) of *D*- and *L*-methyl lactate in (*R*, Δ)- and (*S*, Λ)-CPM films.

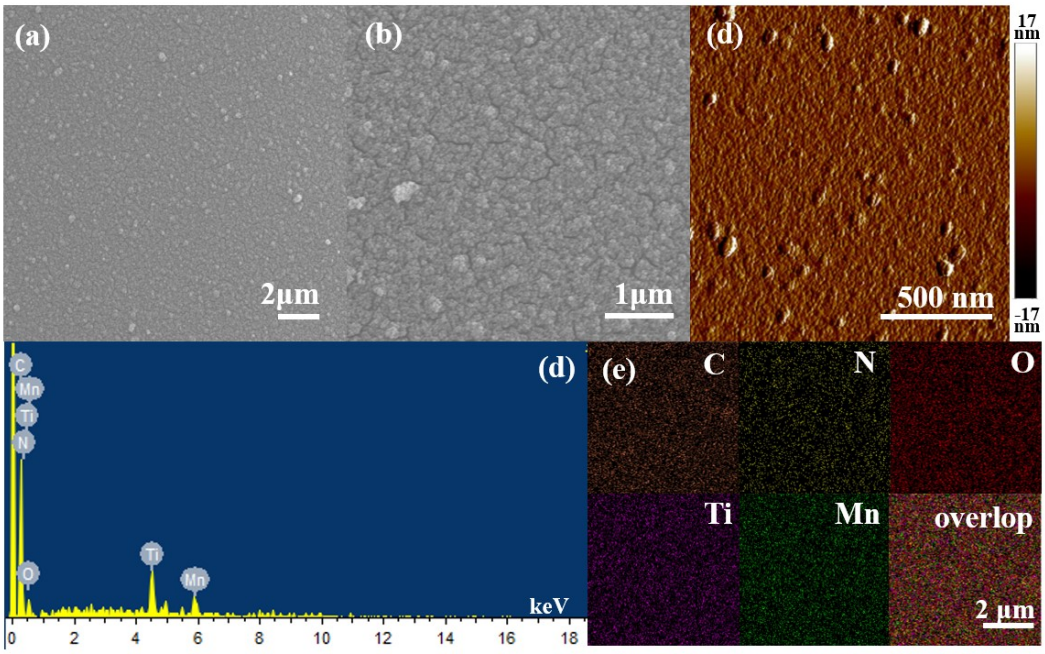

Figure S17. SEM images (a, b), AFM image (c), SEM EDS (d) and element mapping (e) of (*S*, Λ)-CPM film.

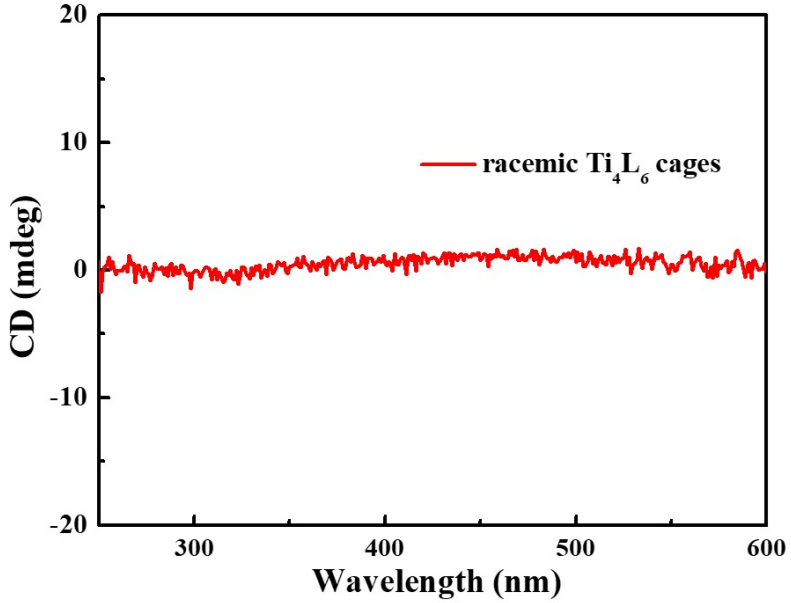

Figure S18. The liquid-state CD spectra of racemic Ti_4L_6 cages in ethanolic solution.